JOURNAL OF GUIDANCE, CONTROL, AND DYNAMICS
Vol. 29, No. 1, January–February 2006

Engineering Notes

ENGINEERING NOTES are short manuscripts describing new developments or important results of a preliminary nature. These Notes should not exceed 2500 words (where a figure or table counts as 200 words). Following informal review by the Editors, they may be published within a few months of the date of receipt. Style requirements are the same as for regular contributions (see inside back cover).

Robust Reorientation and Power Controller Using Flywheels and Control Moment Gyroscopes

Christopher D. Karlgaard*
Analytical Mechanics Associates, Inc., Hampton, Virginia 23666

Introduction

FLYWHEELS are a combined energy and momentum storage device that can offer potential savings in mass for spacecraft by combining both the attitude control and the power management functions. This combination is accomplished by augmenting or altogether replacing conventional batteries and control moment gyroscopes (CMGs). Such systems are commonly known as integrated power and attitude control systems. In Ref. 1, some of the early developments in flywheel technology and applications for combined power and attitude control systems are discussed.

Several research programs have focused on developing a flywheel system for use onboard the ISS. Initially, the flywheels were not designed to aid the ISS double-gimbal CMG-based attitude control system, but were only to provide energy and power management.[2] In Ref. 3, the authors investigated control laws for combining the flywheels with the CMGs for ISS attitude control. The control laws were designed for seeking and maintaining a torque equilibrium attitude (TEA) for flywheel and CMG momentum management and for holding an arbitrary but fixed orientation as would be required for rendezvous and docking operations. Both scenarios made use of linear quadratic regulator (LQR) theory for determining the controller state feedback gains.

The authors of Ref. 3 also considered a nonlinear controller based on Refs. 4 and 5 for performing large-angle reorientation maneuvers. The controller is based on feedback linearization and Lyapunov stability theory and can satisfy control and slew rate limits. The results of applying the nonlinear control law led to singularities in the flywheel steering law such that the power management function of the flywheels could not be accomplished. This problem was remedied by introducing flywheel angular momentum feedback into the control law. An ad hoc procedure was devised in which the same flywheel momentum error feedback gains were used as in the TEA-seeking LQR controller. Numerical simulations of this controller showed good results; however, no stability proof of the controller was presented. It is the purpose of this Note to develop a reorientation controller that is provably globally asymptotically stable and simultaneously manages the flywheel angular momentum to avoid singularities in the power-tracking performance. Additionally, because a structure as large as the ISS is subject to great deal of uncertainty in the knowledge of its inertia, it is desirable that the controller be robust with respect to uncertainties in the inertia properties.[6]

Equations of Motion

In this section, the dynamic model to be used for the nonlinear control law development is discussed. The summary to follow begins with the definition of several coordinate systems.

First, the inertial reference frame is assumed to be located at the center of the Earth and is designated as the I frame. The local-vertical/local-horizontal reference frame, referred to as the L frame, is one in which the $\hat{\boldsymbol{l}}_2$ axis is oriented in the opposite direction of the orbital angular momentum vector, the $\hat{\boldsymbol{l}}_3$ axis points toward the center of the Earth, and the $\hat{\boldsymbol{l}}_1$ axis is chosen to complete a right-handed orthogonal system. Note that for circular orbits $\hat{\boldsymbol{l}}_1$ is in the velocity direction. The reference frame aligned with the body axes of the spacecraft is designated as the B frame. The unit vectors of this frame are $\hat{\boldsymbol{b}}_1$, $\hat{\boldsymbol{b}}_2$, and $\hat{\boldsymbol{b}}_3$. The target/desired reference frame that represents the prescribed final orientation of the body after the reorientation maneuver is designated the D frame, with unit vectors $\hat{\boldsymbol{d}}_1$, $\hat{\boldsymbol{d}}_2$, and $\hat{\boldsymbol{d}}_3$.

The large-angle reorientation attitude kinematics are best represented using the modified Rodrigues parameters (see Ref. 7). The matrix of the transformation from the L frame to B frame is given by[8]

$$\boldsymbol{R}_{LB} = \mathbb{I} + [4(1-\boldsymbol{\beta}^T\boldsymbol{\beta})/(1+\boldsymbol{\beta}^T\boldsymbol{\beta})^2]\boldsymbol{\beta}^\times + [8/(1+\boldsymbol{\beta}^T\boldsymbol{\beta})^2](\boldsymbol{\beta}^\times)^2 \tag{1}$$

where $\boldsymbol{\beta}$ is the modified Rodrigues parameter vector for the transformation between the L frame and the B frame, $\boldsymbol{\beta}^\times$ is given by

$$\boldsymbol{\beta}^\times = \begin{bmatrix} 0 & \beta_3 & -\beta_2 \\ -\beta_3 & 0 & \beta_1 \\ \beta_2 & -\beta_1 & 0 \end{bmatrix} \tag{2}$$

and $\mathbb{I}$ is the identity matrix.

The matrix for the transformation from the L frame to the D frame, $\boldsymbol{R}_{LD}$, is given in terms of the modified Rodrigues parameter $\boldsymbol{\delta}$ and is of the same form as Eq. (1) but is found by using $\boldsymbol{\delta}$ in place of $\boldsymbol{\beta}$. The definition of the preceding transformation matrices lead directly to the definition of an error transformation that describes the difference between the B frame and the D frame. The error transformation matrix, $\boldsymbol{R}_{DB}$, is assumed to be given in terms of the modified Rodrigues parameter $\boldsymbol{\eta}$. The error transformation is given explicitly as $\boldsymbol{R}_{DB} = \boldsymbol{R}_{LB}\boldsymbol{R}_{LD}^T$. The error transformation matrix may also be written in the form of Eq. (1) with parameter $\boldsymbol{\eta}$.

The rotational kinematics of the B frame relative to the D frame are

$$\dot{\boldsymbol{\eta}} = \tfrac{1}{2}\{\mathbb{I} - \boldsymbol{\eta}^\times + \boldsymbol{\eta}\boldsymbol{\eta}^T - [(1+\boldsymbol{\eta}^T\boldsymbol{\eta})/2]\mathbb{I}\}\boldsymbol{\xi} \tag{3}$$

where $\boldsymbol{\xi}$ is the angular velocity of the B frame relative to the D frame, represented in the B frame. The angular velocity of the D frame with respect to the I frame, given by $\boldsymbol{\omega}$, may be written as

$$\boldsymbol{\omega} = 2\boldsymbol{R}_{DB}\left(\mathbb{I} - \boldsymbol{\delta}^\times + \boldsymbol{\delta}\boldsymbol{\delta}^T - \frac{1+\boldsymbol{\delta}^T\boldsymbol{\delta}}{2}\mathbb{I}\right)^{-1}\dot{\boldsymbol{\delta}} - \boldsymbol{R}_{DB}\boldsymbol{R}_{LD}\begin{Bmatrix} 0 \\ \Omega \\ 0 \end{Bmatrix} \tag{4}$$

where Ω is the mean motion of the spacecraft in its orbit.

Received 11 April 2005; revision received 24 June 2005; accepted for publication 25 July 2005.

*Project Engineer, 303 Butler Farm Road, Suite 104A; karlgaard@ama-inc.com. Senior Member AIAA.

The kinetic equation of rotational motion describing the dynamics of the B frame with respect to the D frame may be found from recognizing that the angular velocity of the B frame with respect to the I frame is given by the sum $\boldsymbol{\omega}+\boldsymbol{\xi}$ and that the total angular momentum of the system is the sum $\boldsymbol{I}(\boldsymbol{\omega}+\boldsymbol{\xi})+\boldsymbol{h}+\boldsymbol{H}$, where $\boldsymbol{I}$ is the system inertia matrix, $\boldsymbol{h}$ is the flywheel angular momentum, and $\boldsymbol{H}$ is the CMG angular momentum. Substituting these sums into Euler's rotational equation gives the result[9]

$$\boldsymbol{I}(\dot{\boldsymbol{\omega}}+\dot{\boldsymbol{\xi}})+\dot{\boldsymbol{h}}+\dot{\boldsymbol{H}}+(\boldsymbol{\omega}+\boldsymbol{\xi})^{\times}[\boldsymbol{I}(\boldsymbol{\omega}+\boldsymbol{\xi})+\boldsymbol{h}+\boldsymbol{H}]=\boldsymbol{T} \tag{5}$$

where $\boldsymbol{T}$ is the external torque. The rotational dynamics of the B frame relative to the D frame may be found by solving for $\dot{\boldsymbol{\xi}}$, which yields

$$\dot{\boldsymbol{\xi}}=-\boldsymbol{I}^{-1}[\boldsymbol{I}\dot{\boldsymbol{\omega}}+\boldsymbol{\xi}^{\times}\boldsymbol{I}\boldsymbol{\xi}+\boldsymbol{\omega}^{\times}\boldsymbol{I}\boldsymbol{\omega}+\boldsymbol{\omega}^{\times}\boldsymbol{I}\boldsymbol{\xi}+\boldsymbol{\xi}^{\times}\boldsymbol{I}\boldsymbol{\omega}+\boldsymbol{I}\boldsymbol{\xi}^{\times}\boldsymbol{\omega}-\boldsymbol{T}+\boldsymbol{\tau}+\boldsymbol{\sigma}] \tag{6}$$

where $\boldsymbol{\tau}$ is the CMG internal torque and $\boldsymbol{\sigma}$ is the flywheel internal torque, which are defined as

$$\boldsymbol{\sigma}=\dot{\boldsymbol{h}}+(\boldsymbol{\omega}+\boldsymbol{\xi})^{\times}\boldsymbol{h} \tag{7}$$

$$\boldsymbol{\tau}=\dot{\boldsymbol{H}}+(\boldsymbol{\omega}+\boldsymbol{\xi})^{\times}\boldsymbol{H} \tag{8}$$

Assuming, without loss of generality, that the flywheel system is made up of rotors arranged in counter-rotating pairs in each of the body-axis directions, implies that the rotational equations for the wheel speeds are[3,10]

$$J\dot{v}_1=M_1-J\dot{\xi}_1 \tag{9}$$

$$J\dot{v}_2=M_2-J\dot{\xi}_1 \tag{10}$$

$$J\dot{v}_3=M_3-J\dot{\xi}_2 \tag{11}$$

$$J\dot{v}_4=M_4-J\dot{\xi}_2 \tag{12}$$

$$J\dot{v}_5=M_5-J\dot{\xi}_3 \tag{13}$$

$$J\dot{v}_6=M_6-J\dot{\xi}_3 \tag{14}$$

where M_i is the motor–generator torque, v_1 and v_2 are the speeds of the two flywheel rotors aligned with the $\hat{\boldsymbol{b}}_1$ axis, and similarly for the other pairs of rotors for the $\hat{\boldsymbol{b}}_2$ and $\hat{\boldsymbol{b}}_3$ axes, and J is the flywheel rotational inertia.

The external torque $\boldsymbol{T}$ includes all disturbances. For this Note, only the gravity torque is modeled explicitly. The gravity torque may be expressed as

$$\boldsymbol{T}=3\Omega^2\hat{\boldsymbol{\lambda}}^{\times}\boldsymbol{I}\hat{\boldsymbol{\lambda}} \tag{15}$$

where the quantity $\hat{\boldsymbol{\lambda}}$ is the representation of the $\hat{\boldsymbol{l}}_3$ axis in the B frame, found from $\hat{\boldsymbol{\lambda}}=\boldsymbol{R}_{LB}\hat{\boldsymbol{l}}_3$.

Note that the inertia properties of the spacecraft are realistically not known with precise certainty. Therefore, the inertia matrix may be expanded as $\boldsymbol{I}=\boldsymbol{I}_0+\boldsymbol{\Lambda}$, where $\boldsymbol{I}_0$ is the known or nominal inertia matrix, and $\boldsymbol{\Lambda}$ represents the difference between the actual and nominal inertia. Clearly $\boldsymbol{\Lambda}$ is an unknown quantity, although it will be assumed later that the uncertainty has a known bound.

In summary, the rotational equations of motion to be controlled may be written in the form

$$\dot{\boldsymbol{\eta}}=\boldsymbol{G}(\boldsymbol{\eta})\boldsymbol{\xi} \tag{16}$$

$$\begin{Bmatrix}\dot{\boldsymbol{\xi}}\\ \dot{\boldsymbol{h}}\end{Bmatrix}=\boldsymbol{f}_a(\boldsymbol{\eta},\boldsymbol{\xi},\boldsymbol{h},t)+\boldsymbol{G}_a\begin{Bmatrix}\boldsymbol{\tau}+\boldsymbol{\mu}(\boldsymbol{\eta},\boldsymbol{\xi},\boldsymbol{\tau},\boldsymbol{\sigma},t)\\ \boldsymbol{\sigma}\end{Bmatrix} \tag{17}$$

where

$$\boldsymbol{G}(\boldsymbol{\eta})=\tfrac{1}{2}\{\mathbb{I}-\boldsymbol{\eta}^{\times}+\boldsymbol{\eta}\boldsymbol{\eta}^{T}-[(1+\boldsymbol{\eta}^{T}\boldsymbol{\eta})/2]\mathbb{I}\} \tag{18}$$

$$\boldsymbol{f}_a(\boldsymbol{\eta},\boldsymbol{\xi},\boldsymbol{h},t)=\begin{Bmatrix}-\boldsymbol{I}_0^{-1}\big[\boldsymbol{I}_0\dot{\boldsymbol{\omega}}+\boldsymbol{\xi}^{\times}\boldsymbol{I}_0\boldsymbol{\xi}+\boldsymbol{\omega}^{\times}\boldsymbol{I}_0\boldsymbol{\omega}+\boldsymbol{\omega}^{\times}\boldsymbol{I}_0\boldsymbol{\xi}+\boldsymbol{\xi}^{\times}\boldsymbol{I}_0\boldsymbol{\omega}\\ \quad+\boldsymbol{I}_0\boldsymbol{\xi}^{\times}\boldsymbol{\omega}-3\Omega^2\hat{\boldsymbol{l}}_3^{\times}\boldsymbol{I}_0\hat{\boldsymbol{l}}_3\big]\\ -(\boldsymbol{\omega}+\boldsymbol{\xi})^{\times}\boldsymbol{h}\end{Bmatrix} \tag{19}$$

$$\boldsymbol{G}_a=\begin{bmatrix}-\boldsymbol{I}_0^{-1} & -\boldsymbol{I}_0^{-1}\\ 0 & \mathbb{I}\end{bmatrix} \tag{20}$$

$$\boldsymbol{\mu}(\boldsymbol{\eta},\boldsymbol{\xi},\boldsymbol{\tau},\boldsymbol{\sigma},t)=\big[\boldsymbol{I}_0\dot{\boldsymbol{\omega}}+\boldsymbol{\xi}^{\times}\boldsymbol{I}_0\boldsymbol{\xi}+\boldsymbol{\omega}^{\times}\boldsymbol{I}_0\boldsymbol{\omega}+\boldsymbol{\omega}^{\times}\boldsymbol{I}_0\boldsymbol{\xi}+\boldsymbol{\xi}^{\times}\boldsymbol{I}_0\boldsymbol{\omega}+\boldsymbol{I}_0\boldsymbol{\xi}^{\times}\boldsymbol{\omega}-3\Omega^2\hat{\boldsymbol{l}}_3^{\times}\boldsymbol{I}_0\hat{\boldsymbol{l}}_3\big]-\boldsymbol{I}_0\mathbb{I}^{-1}\big[\boldsymbol{I}\dot{\boldsymbol{\omega}}+\boldsymbol{\xi}^{\times}\boldsymbol{I}\boldsymbol{\xi}+\boldsymbol{\omega}^{\times}\boldsymbol{I}\boldsymbol{\omega}+\boldsymbol{\omega}^{\times}\boldsymbol{I}\boldsymbol{\xi}+\boldsymbol{\xi}^{\times}\boldsymbol{I}\boldsymbol{\omega}+\boldsymbol{I}\boldsymbol{\xi}^{\times}\boldsymbol{\omega}-3\Omega^2\hat{\boldsymbol{l}}_3^{\times}\boldsymbol{I}\hat{\boldsymbol{l}}_3\big]+\big[\mathbb{I}-\boldsymbol{I}_0\boldsymbol{I}^{-1}\big](\boldsymbol{\tau}+\boldsymbol{\sigma}) \tag{21}$$

where $\boldsymbol{\mu}$ represents the uncertainty in the rotational dynamics of the B frame due to imperfect knowledge of the inertia matrix. Note that $\boldsymbol{I}_0=\boldsymbol{I}$ implies that $\boldsymbol{\mu}=\boldsymbol{0}$.

In summary, the kinematic differential equations describing the evolution of the B frame relative to the D frame, as paramterized by $\boldsymbol{\eta}$, is given in Eq. (16) and the kinetic differential equations describing the dynamics of the angular velocity of the B frame relative to the D frame and the flywheel angular momentum is given in Eq. (17). The control design problem seeks to determine inputs $\boldsymbol{\tau}$ and $\boldsymbol{\sigma}$ such that $\boldsymbol{\eta}$, $\boldsymbol{\xi}$, and $\boldsymbol{h}$ go to zero asymptotically, for generic initial conditions. The CMG momentum is governed by Eq. (8) and is not expected to go to zero during the reorientation maneuver. The control design problem is further constrained by the flywheel power management function, as is discussed in the next section.

Power Management with Flywheels

A further constraint on the problem is that the flywheel system must simultaneously provide the requisite control torque $\boldsymbol{\sigma}$ as well as the total electrical power as required by the spacecraft bus. The power provided by the flywheels is given by[3]

$$P=J(\dot{v}_1v_1+\dot{v}_2v_2+\dot{v}_3v_3+\dot{v}_4v_4+\dot{v}_5v_5+\dot{v}_6v_6) \tag{22}$$

If the components of the spacecraft inertial angular velocity are assumed to be small relative to the flywheel speeds, then the motor–generator torque required to effect the control torque may be approximated by $M_i=J\dot{v}_i$, for $i=1,\ldots,6$. Assembling the preceding equations together results in an underdetermined system of the form $\boldsymbol{A}\boldsymbol{x}=\boldsymbol{y}$, where

$$\boldsymbol{A}=\begin{bmatrix}1 & 1 & 0 & 0 & 0 & 0\\ 0 & 0 & 1 & 1 & 0 & 0\\ 0 & 0 & 0 & 0 & 1 & 1\\ v_1 & v_2 & v_3 & v_4 & v_5 & v_6\end{bmatrix} \tag{23}$$

$$\boldsymbol{x}=[M_1 \quad M_2 \quad M_3 \quad M_4 \quad M_5 \quad M_6]^T \tag{24}$$

$$\boldsymbol{y}=[\boldsymbol{\sigma}+(\boldsymbol{\omega}+\boldsymbol{\xi})^{\times}\boldsymbol{h}, \quad P]^T \tag{25}$$

One solution of the system of equations is the Moore–Penrose matrix pseudoinverse, which yields the minimum-norm solution for the motor–generator torque. The solution is $\boldsymbol{x}=\boldsymbol{A}^T(\boldsymbol{A}\boldsymbol{A}^T)^{-1}\boldsymbol{y}$. An analytic expression for the matrix pseudoinverse is given in Refs. 3 and 10 and is not repeated here.

Controller Design

In this section, the development of a control law for performing large-angle reorientation maneuvers and simultaneous flywheel momentum and power management using the sliding mode technique is described. The equations of motion given in Eqs. (16) and (17) are well suited for a sliding mode control design,[11] which is essentially a robust backstepping technique. Backstepping is a systematic control design method in which a subset of the state space is regarded as an input to the dynamics of another subset of the state space. This pseudoinput is designed to stabilize asymptotically the subset of the dynamics. The next step of the control design procedure is to pick the next series of inputs to make the previous pseudoinputs track to the desired value. The process is then applied in recursion through all subsets of the dynamics until the actual control input is designed. Sliding mode control is a robust approach in which the controller compensates for structured uncertainty in the system dynamics.[11] The control design technique is similar to backstepping in the sense that the model takes the form of a cascaded nonlinear system, but

differs in that the error between the actual and desired pseudoinputs is made to converge to zero (or a neighborhood of zero) in finite time rather than asymptotically. Backstepping and sliding mode control techniques have been applied to spacecraft reorientation problems in Refs. 12–14.

In the spacecraft reorientation problem at hand, there are two subsystems to work with. First is the $\boldsymbol{\eta}$ subsystem for which $\boldsymbol{\xi}$ is to be considered as an input. The second subsystem is the $(\boldsymbol{\xi}, \boldsymbol{h})$ subsystem for which the control inputs $\boldsymbol{\tau}$ and $\boldsymbol{\sigma}$ are to be designed to meet the requirements set forth on $\boldsymbol{\xi}$ in the first problem.

Kinematic Subsystem

To find a choice of $\boldsymbol{\xi} = \boldsymbol{\phi}(\boldsymbol{\eta})$ to stabilize the $\boldsymbol{\eta}$ dynamics, consider the function[7] $V(\boldsymbol{\eta}) = 2\,\ell_n(1 + \boldsymbol{\eta}^T\boldsymbol{\eta})$. This function is both positive definite and radially unbounded. Also, $V = 0$ only when $\boldsymbol{\eta} = 0$. A choice of feedback $\boldsymbol{\phi}(\boldsymbol{\eta}) = -\boldsymbol{K}_1\boldsymbol{\eta}$, where $\boldsymbol{K}_1 > 0$, renders the function rate $\dot{V} = -\boldsymbol{\eta}^T\boldsymbol{K}_1\boldsymbol{\eta} < 0$, as has been shown in Ref. 7. With this choice of feedback, the subsystem is globally asymptotically stable from Lyapunov's direct method (Theorem 4.2 in Ref. 11). Additionally, the kinematics have no uncertainty, and therefore, the closed-loop system with this choice of pseudoinput can be thought of as robust.

Kinetic Subsystem

To design a controller to drive the $(\boldsymbol{\xi}, \boldsymbol{h})$ dynamics to the desired value of the pseudoinputs $[\boldsymbol{\phi}(\boldsymbol{\eta}), \boldsymbol{0}]$ in finite time, first define the error as $\boldsymbol{z} = \{\boldsymbol{\xi} - \boldsymbol{\phi}(\boldsymbol{\eta}), \boldsymbol{h}\}^T$, which obeys the dynamics

$$\dot{\boldsymbol{z}} = \boldsymbol{f}_a(\boldsymbol{\eta}, \boldsymbol{\xi}, \boldsymbol{h}) + \boldsymbol{G}_a \begin{Bmatrix} \boldsymbol{\tau} + \boldsymbol{\mu}(\boldsymbol{\eta}, \boldsymbol{\xi}, \boldsymbol{\tau}, \boldsymbol{\sigma}) \\ \boldsymbol{\sigma} \end{Bmatrix} - \begin{Bmatrix} \dfrac{\partial \boldsymbol{\phi}}{\partial \boldsymbol{\eta}} \boldsymbol{G}(\boldsymbol{\eta})\boldsymbol{\xi} \\ \boldsymbol{0} \end{Bmatrix} \tag{26}$$

When the preliminary controller

$$\begin{Bmatrix} \boldsymbol{\tau} \\ \boldsymbol{\sigma} \end{Bmatrix} = \boldsymbol{G}_a^{-1} \left[\begin{Bmatrix} \dfrac{\partial \boldsymbol{\phi}}{\partial \boldsymbol{\eta}} \boldsymbol{G}(\boldsymbol{\eta})\boldsymbol{\xi} \\ \boldsymbol{0} \end{Bmatrix} - \boldsymbol{f}_a(\boldsymbol{\eta}, \boldsymbol{\xi}, \boldsymbol{h}) \right] + \boldsymbol{G}_a^{-1} \begin{Bmatrix} \tilde{\boldsymbol{\tau}} \\ \tilde{\boldsymbol{\sigma}} \end{Bmatrix} \tag{27}$$

is substituted, the error dynamics transform to

$$\dot{\boldsymbol{z}} = \begin{Bmatrix} \tilde{\boldsymbol{\tau}} \\ \tilde{\boldsymbol{\sigma}} \end{Bmatrix} + \boldsymbol{G}_a \begin{Bmatrix} \boldsymbol{\mu}(\boldsymbol{\eta}, \boldsymbol{\xi}, \boldsymbol{\tau}, \boldsymbol{\sigma}) \\ \boldsymbol{0} \end{Bmatrix} \tag{28}$$

If the function ρ and parameter k are defined as

$$\rho(\boldsymbol{\eta}, \boldsymbol{\xi}, \boldsymbol{h}) = \left\| \boldsymbol{I}_0^{-1} \right\|_\infty^2 \|\boldsymbol{\Lambda}\|_\infty^2 [\|\boldsymbol{\xi}\|^2 + \|\boldsymbol{\omega}\|^2 + \|\dot{\boldsymbol{\omega}}\| + 3\|\boldsymbol{\xi}\|\|\boldsymbol{\omega}\| + 3\Omega^2] \tag{29}$$

$$k = \left\| \boldsymbol{I}_0^{-1} \right\|_\infty^2 \|\boldsymbol{\Lambda}\|_\infty + \left\| \boldsymbol{I}_0^{-1} \right\|_\infty \tag{30}$$

Then it may be shown that the uncertainty term in the preceding differential equation obeys the bound

$$\left\| \boldsymbol{G}_a \begin{Bmatrix} \boldsymbol{\mu}(\boldsymbol{\eta}, \boldsymbol{\xi}, \boldsymbol{\tau}, \boldsymbol{\sigma}, t) \\ \boldsymbol{0} \end{Bmatrix} \right\|_\infty \leq \rho(\boldsymbol{\eta}, \boldsymbol{\xi}, \boldsymbol{h}) + k \left\| \begin{Bmatrix} \tilde{\boldsymbol{\tau}} \\ \tilde{\boldsymbol{\sigma}} \end{Bmatrix} \right\|_\infty \tag{31}$$

Note that the term $\|\boldsymbol{\Lambda}\|_\infty$ is meant to be a measure of the known bound on the inertia uncertainty, not the norm of the actual inertia deviation, which remains unknown.

The controller that drives the error state $\boldsymbol{z}$ to zero (or a neighborhood of zero, as will be discussed presently) is given by[11]

$$\begin{Bmatrix} \tilde{\boldsymbol{\tau}} \\ \tilde{\boldsymbol{\sigma}} \end{Bmatrix} = -\frac{1}{1-k} \begin{Bmatrix} [\rho(\boldsymbol{\eta}, \boldsymbol{\xi}, \boldsymbol{h}) + b_\xi]\,\mathrm{sat}\,[\boldsymbol{\xi} - \boldsymbol{\phi}(\boldsymbol{\eta}), \epsilon] \\ [\rho(\boldsymbol{\eta}, \boldsymbol{\xi}, \boldsymbol{h}) + b_h]\,\mathrm{sat}\,(\boldsymbol{h}, \epsilon) \end{Bmatrix} \tag{32}$$

where b_ξ and b_h are parameters that define the desired convergence time and the saturation function is defined as

$$\mathrm{sat}\,(\zeta, \epsilon) = \begin{cases} 1 & \text{for} \quad \zeta > \epsilon \\ \zeta/\epsilon & \text{for} \quad |\zeta| \leq \epsilon \\ -1 & \text{for} \quad \zeta < -\epsilon \end{cases} \tag{33}$$

for some input ζ. The use of the saturation function rather that the sign function guarantees convergence of $\boldsymbol{z}$ to a neighborhood of $\boldsymbol{0}$ (Ref. 11), but avoids problems associated with discontinuous control inputs. (Note that the saturation function and the sign function are equivalent for $\epsilon = 0$.) In the next section, numerical simulation of the controller designed in this section is discussed.

Numerical Simulation

In this section, simulation results of the equations of motion and feedback controller discussed in the preceding sections are provided. Initial conditions and simulation parameters are summarized in

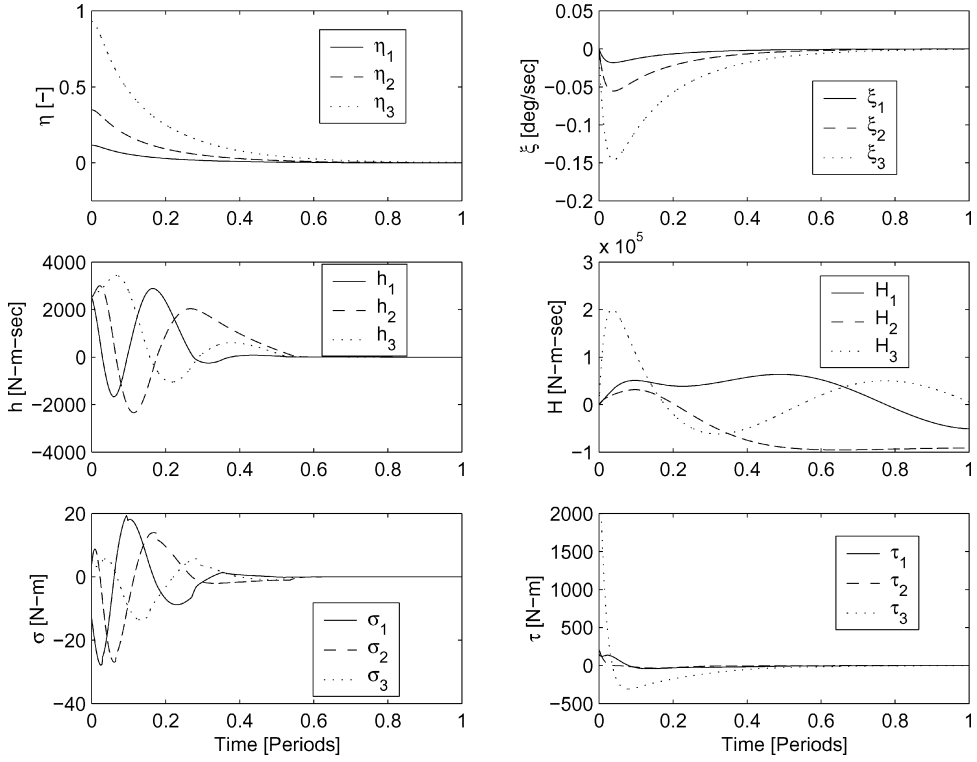

Fig. 1 Simulation results.

Table 1 Simulation and control parameters

Parameter	Value
Ω	1.131×10^{-3} rad/s
$\boldsymbol{\delta}$	$[0, 0, 0]^T$
$\boldsymbol{\eta}(0)$	$[0.116, 0.349, 0.930]^T$
$\boldsymbol{\xi}(0)$	$[0, 0, 0]^T$
$v_1(0)$, $v_3(0)$, $v_5(0)$	25.0 krpm
$v_2(0)$, $v_4(0)$, $v_6(0)$	20.0 krpm
J	$4.82\ \text{kg} \cdot \text{m}^2$
$\|\boldsymbol{\Lambda}\|_\infty$	$1{,}616{,}496\ \text{kg} \cdot \text{m}^2$
b_ξ	10^{-4}
b_h	1
k	7.65×10^{-8}
ϵ	0.01

Table 1. Additionally, the inertia matrices, gain matrices, and desired power profile used for simulation are as follows:

$$\boldsymbol{I}_0 = (1.36 \times 10^6) \begin{bmatrix} 50.28 & -0.39 & -0.24 \\ -0.39 & 10.80 & 0.16 \\ -0.24 & 0.16 & 58.57 \end{bmatrix} \tag{34}$$

$$\boldsymbol{I} = (1.36 \times 10^6) \begin{bmatrix} 50.18 & -0.37 & -0.22 \\ -0.37 & 10.71 & 0.11 \\ -0.22 & 0.11 & 59.10 \end{bmatrix} \tag{35}$$

$$\boldsymbol{K}_1 = (1/250)\mathbb{I} \tag{36}$$

$$P = \begin{cases} 105.6\ \text{kW} & \text{for} \quad 0 < t \le \frac{2}{3}(2\pi/\Omega) \\ -211.2\ \text{kW} & \text{for} \quad \frac{2}{3}(2\pi/\Omega) < t \le 2\pi/\Omega \end{cases} \tag{37}$$

The results of the controller implementation are shown in Fig. 1. Figure 1 shows the time histories of the modified Rodrigues parameters $\boldsymbol{\eta}$ and the time histories of the angular velocity of the B frame relative to the D frame, $\boldsymbol{\xi}$. The angular velocity rapidly reaches the desired value $\phi(\boldsymbol{\eta})$, and from there, the orientation error decays to the origin asymptotically. The flywheel momentum and CMG momentum are shown in Fig. 1. The flywheel momentum is clearly stabilized, although with some overshoot, which could be eliminated with an increased gain. Finally, the control torques as output from the feedback law are shown in Fig. 1. Note that the CMG control torque is larger than the flywheel control torque by several orders. The flywheel motor–generator torques determined from the desired power profile and the desired control torque are not shown, nor are the flywheel speeds.

Conclusions

The formulation and implementation of a nonlinear controller for performing large-angle reorientation maneuvers have been discussed. The controller exploited the cascaded structure of the dynamics and was designed explicitly to be robust with respect to poor knowledge of the spacecraft inertia properties. The results show adequate performance of the controller, although some tuning of gains would be required to achieve some specific objectives, in terms of settling time and overshoot, for example. Additionally, future work could focus on developing Monte Carlo simulations of the proposed controllers to evaluate robustness properties for comparison with design specifications.

References

[1]Tsiotras, P., Shen, H., and Hall, C., "Satellite Attitude Control and Power Tracking with Energy/Momentum Wheels," *Journal of Guidance, Control, and Dynamics*, Vol. 24, No. 1, 2001, pp. 23–34.

[2]Roithmayr, C. M., "International Space Station Attitude Control and Energy Storage Experiment: Effects of Flywheel Torque," NASA TM-1999-209100, Feb. 1999.

[3]Roithmayr, C. M., Karlgaard, C. D., Kumar, R. R., Seywald, H., and Bose, D. M., "Dynamics and Control of Attitude, Power, and Momentum for a Spacecraft Using Flywheels and Control Moment Gyroscopes," NASA TP-2003-212178, April 2003.

[4]Seywald, H., Lim, K. B., Kumar, R. R., and Anthony, T. C., "Stability Analysis for Constrained Principal Axis Slew Maneuvers," *Journal of the Astronautical Sciences*, Vol. 47, Nos. 3 and 4, 1999, pp. 239–258.

[5]Seywald, H., "Globally Asymptotically Stable Reorientation Controller with Control Constraint and Slew Rate Limit," *Journal of the Astronautical Sciences*, Vol. 48, No. 1, 2000, pp. 45–67.

[6]Wie, B., Hu, A., and Singh, R., "Multibody Interaction Effects on Space Station Attitude Control and Momentum Management," *Journal of Guidance, Control, and Dynamics*, Vol. 13, No. 6, 1990, pp. 993–999.

[7]Tsiotras, P., "Stabilization and Optimality Results for the Attitude Control Problem," *Journal of Guidance, Control, and Dynamics*, Vol. 19, No. 4, 1996, pp. 772–779.

[8]Shuster, M. D., "A Survey of Attitude Representations," *Journal of the Astronautical Sciences*, Vol. 41, No. 4, 1993, pp. 439–518.

[9]Wie, B., Bailey, D., and Heiberg, C., "Singularity Robust Steering Logic for Redundant Single-Gimbal Control Moment Gyros," *Journal of Guidance, Control, and Dynamics*, Vol. 24, No. 5, 2001, pp. 865–872.

[10]Roithmayr, C. M., Karlgaard, C. D., Kumar, R. R., and Bose, D. M., "Integrated Power and Attitude Control with Spacecraft Flywheels and Control Moment Gyroscopes," *Journal of Guidance, Control, and Dynamics*, Vol. 27, No. 5, 2004, pp. 859–873.

[11]Khalil, H. K., *Nonlinear Systems*, 3rd ed., Prentice–Hall, Upper Saddle River, NJ, 2002, pp. 111–156.

[12]Chen, Y.-P., and Lo, S.-C., "Sliding Mode Controller Design for Spacecraft Attitude Tracking Maneuvers," *IEEE Transactions on Aerospace and Electronic Systems*, Vol. 29, No. 4, 1993, pp. 1328–1333.

[13]Crassidis, J. L., and Markley, F. L., "Sliding Mode Control Using Modified Rodrigues Parameters," *Journal of Guidance, Control, and Dynamics*, Vol. 19, No. 6, 1996, pp. 1381–1383.

[14]Kim, K.-S., and Kim, Y., "Robust Backstepping Control for Slew Maneuver Using Nonlinear Tracking Function," *IEEE Transactions on Control Systems Technology*, Vol. 11, No. 6, 2003, pp. 822–829.